Petro-physical characterization of shallow aquifers by using AVO and theoretical approaches

U. Tinivella, F. Accaino, M. Giustiniani and S. Picotti

Istituto Nazionale di Oceanografia e di Geofisica Sperimentale, Trieste, Italy

(Received: August 12, 2007; accepted: September 10, 2007)

ABSTRACT We present the results obtained by the Amplitude Versus Offset analysis of 2D and 3D high-resolution seismic data acquired along the resurgence line located in the Friuli-Venezia Giulia plain (NE Italy), in order to characterize an important multilayered aquifer. The Amplitude Versus Offset analysis was performed to extract the Poisson ratio contrast, which provides useful information to characterize the aquifers petro-physical properties, such as the fluid content.The velocity model, which was obtained from a tomographic approach for 2D seismic data and an iterative updating procedure involving pre-stack depth migration, residual move-out analysis and seismic reflection tomography for 3D data, was used to obtain density and porosity maps.

1. Introduction

In the frame of the CAMI project, 2D and 3D seismic data were acquired to characterize the aquifer system located in the Torrate area (Friuli-Venezia Giulia region in north-eastern Italy). During the winter of 2005, three 2D seismic lines were acquired, as described in Giustiniani *et al.* (2009). In addition, 3D seismic surveys were performed in two different seasons and in two different areas as described in Picotti *et al.* (2009).

Firstly, we tested the possibility of detecting the pore pressure variation in different seasons, in the acquifer system, by seismic velocity and Amplitude Versus Offset (AVO) analyses. We used an empirical approach (Prasad *et al.*, 2004) to determine the seismic velocities versus pore pressure.

After "true-amplitude" processing of both 2D and 3D seismic data (Giustiniani *et al.*, 2009; Picotti *et al.*, 2009), the AVO was applied to all seismic data sets in order to extract the Poisson ratio contrast that which provides useful information about the petro-physical properties of the shallow layers.

The velocity fields were obtained from a tomographic approach for 2D seismic data (Giustiniani *et al.*, 2009) and an iterative procedure for 3D seismic data (Picotti *et al.*, 2009). They were translated, in terms of porosity and density, by using empirical relationships.

2. Velocity and AVO vs. pore pressure

Velocities versus pore pressure have been computed in order to verify the possibility of detecting overpressures through seismic data analysis for the shallower aquifers, one located at about a 30 m depth while the second one at about a 180 m depth. The identified physical properties of these aquifers are reported in Table 1 (layers 2 and 4). Laboratory measurements

indicate the following relationship between compressional (V_P) and shear (V_S) wave velocities and effective pressure p_e (Prasad *et al.*, 2004):

$$V_P = a_1 + b_1 p_e^{c_1}, \quad V_S = a_2 p_e^{b_2} \tag{1}$$

where the coefficients a_i and b_i are obtained by fitting the model parameters (Table 1) and c_i was fixed equal to the value proposed by Prasad *et al.* (2004). The fit gives the results shown in Table 2. Considering a 10% increase in hydrostatic pressure of each aquifer obtained from well measurements performed by the waterworks technicians (Enrico Marin, personal communication), we evaluated the compressional and shear velocities and the density values shown in Table 1. The velocity variation caused by conditions of overpressure is not detectable by seismic methods. On the other hand, the ratio between the V_P and V_S reflectivity, which can be estimated by the AVO analysis, can detect the top and the bottom of each layer (Fig. 1), where the reflectivity (R_X) of the X parameter is defined as:

$$R_X = \frac{\Delta X}{\overline{X}}, \tag{2}$$

where ΔX is the variation of the X parameter and $\overline{X}$ is its average value at the interface, as indicated by the upper bar.

In the case of conditions of overpressure, the V_P to V_S reflectivity ratio is slightly modified, except at the bottom of the second aquifer (Fig. 1). In fact, in hydrostatic conditions, we assumed

Table 1 - Seismic properties of the aquifer model shown in Fig. 2: compressional-wave (P) and shear-wave (S) velocities, density, and quality factors (Bourbié *et al.*, 1987; Prasad and Meissner, 1992; Schön, 1996). The values in brackets refer to the overpressure condition (see text). The seismic parameters of layer 6 (velocity and density) are linearly interpolated.

Layer	Medium	Mean thickness	V_P (m/s)	V_S (m/s)	ρ (kg/m^3)	Q_P	Q_S
1	Clay+gravel	27	1000	300	1700	20	20
2	Saturated gravel	55	1600 (1564)	450 (427)	1900 (1890)	40 (40)	40 (40)
3	Clay	178	1800	600	2000	30	30
4	Saturated gravel	200	2200 (2142)	800 (767)	2100 (2080)	50 (50)	50 (50)
5	Clay	400	2000	700	2200	40	40
6	Gravel+sand+clay (top)	850	1800	600	1900	60	60
	Gravel+sand+clay (bottom)		2500	1000	2300	60	60
7	Carbonatic basement		3500	1900	2800	100	100

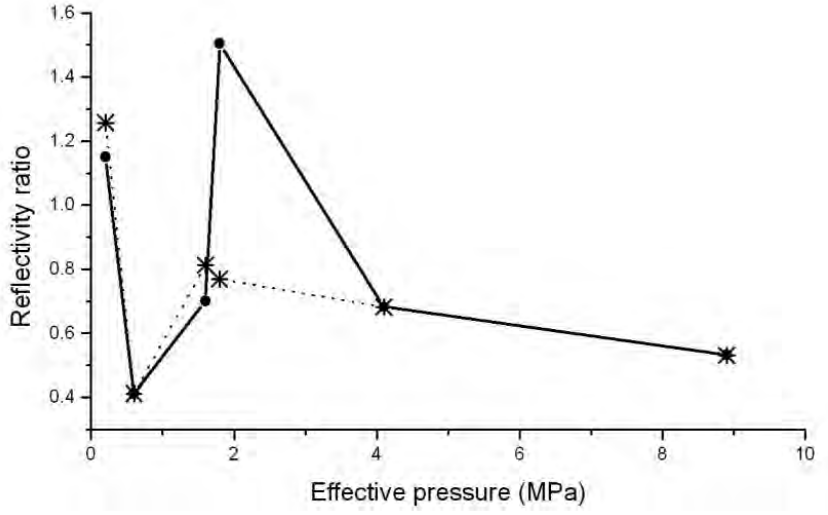

Fig. 1 - V_P and V_S reflectivity ratio versus effective pressure at each modelled layer (see values in Table 1). Circle: hydrostatic condition; star: overpressure condition.

a velocity inversion between the second aquifer and the underlying layer (Table 1). In conditions of overpressure, the velocity contrast reduces itself; consequently, the V_P and V_S reflectivity ratio decreases, these masking the bottom of the second aquifer. So, in this case, the AVO analysis highlights possible lithological and saturation changes in porous media.

3. Amplitude Versus Offset

3.1. The analysis

The pre-stack data analysis underlines the presence of AVO effects associated either with lithologic changes or/and the presence of fluids at high pressure. These effects are evident, for example, in the three stacked sections of Line 2 obtained by using different offset ranges: 0 -199 m, 200 – 399 m, and higher than 400 m (Fig. 2). This figure shows that the amplitudes at the two main shallow aquifers change with offset. In the far-offset section, the amplitude is stronger compared to the others: this is evident for the deeper reflectors, at about 300 m and 500 m. As expected, the near-offset stacked section provides more information about the shallowest targets.

To better discriminate between lithologic and fluid changes at each interface, we performed the AVO analysis by using commercial software (Vern and Hilterman, 1995). We linearized Zoeppritz's equations using the Aki-Richards method (Aki and Richards, 1980). This approach

Table 2 - Fitting parameters of the Eq. (1).

index	a	b
1	973.4	985.2
2	662.6	0.349

considers the linearization of the equations with respect to the P-wave velocity reflectivity (mainly influenced by the near offsets), the S-wave velocity reflectivity (mainly influenced by the medium-large offsets), and the density reflectivity (related to the very large offsets). The AVO equation of the P-wave reflection coefficient $R(\theta)$ versus the incidence angle θ, following the Aki and Richards (1980) approximation, is given by the following equation, where only the angles lower than the critical angle are considered:

$$R(\theta) = \frac{A_1}{A_0} = \left[\frac{1}{2}\left(1 + \tan^2\theta\right)\right] R_{V_P} - \left[4\,\frac{\overline{V}_S^2}{\overline{V}_P^2}\sin^2\theta\right] R_{V_S} + \left[\frac{1}{2}\left(1 - 4\,\frac{\overline{V}_S^2}{\overline{V}_P^2}\sin^2\theta\right)\right] R_\rho \qquad (3)$$

where A is the P-wave amplitude, the index 0 and 1 indicate the incidence and reflected waves respectively. Given the reflection coefficients at distinct offsets, a ray tracing was performed through the background velocity model to obtain the angles of incidence at all desired reflectors. Although, for perfect data, the solution for all three reflectivities (R_{VP}, R_{VS} and R_ρ) is attainable in practice, on numerical grounds (e.g. matrix stability, limited aperture, noise, and incomplete amplitude recovery), R_ρ estimation is unstable. Therefore, the density is represented empirically, in terms of P-wave velocity, by using the Gardner formula (Gardner *et al.*, 1974) and AVO determines the R_{VP} and the R_{VS} parameters only. Then, the AVO inversion process calculates the elastic parameters, and we obtained, in the time domain, two sections that give details on the normalized change in P- and S-wave velocities: the R_{VP} and the R_{VS} sections. Recalling the fact that the P-wave velocity depends on both fluid and solid properties and the S-wave velocity depends mainly on the solid properties, the joint analysis of the two AVO sections gives information about the nature of the main reflections. If a reflection is present in both sections, it is mainly caused by change of the solid properties at the interface, i.e. by lithological changes. If a reflection is identified only in the P-wave reflectivity section, instead, the contrast of P-wave velocity, without any change of the S-wave velocity, can be justified assuming that the fluid content changes at the interface.

The inputs of the amplitude inversion are:

(i) the data processed following a true-amplitude scheme [see details in Giustiniani *et al.* (2009)],

(ii) the acquisition geometry used to apply a correction for source and receiver directivities, and

(iii) the velocity model obtained by the tomographic inversion [see details in Picotti *et al.* (2009)].

The velocity model allows us to calculate the ray path and converting the offsets to angles of incidence. We analysed the amplitude variations versus angle of incidence and obtained sections of both P- and S-wave velocity reflectivity. The ratios between the P- and S-wave reflectivity are related to Poisson's ratio and, consequently, to the fluid content.

After the visual comparison of the reflectivity sections, we decided to use a quantitative method to interpret the AVO results. We evaluated the ratio between P and S reflectivity (Accaino *et al.*, 2005).

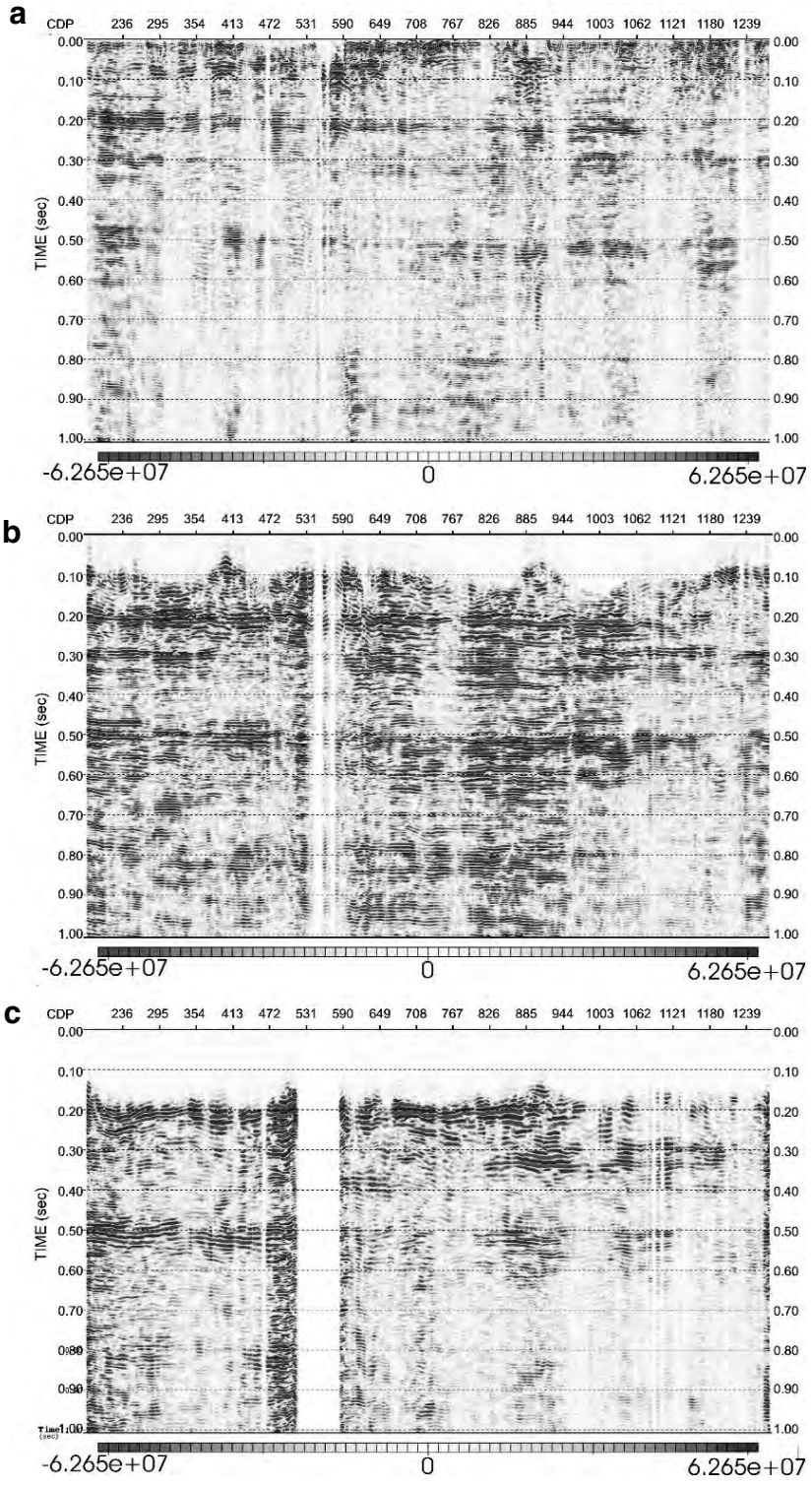

Fig. 2 - Stack section of Line 2 by using the traces with an offset ranging between 2.5 m and 199 m (a), between 200 m and 399 m (b) and greater than 400 m (c). The seismic sections are aligned in function of the CDP ranging between 177 and 1276. The gap in the panel c is related to a geometrical acquisition.

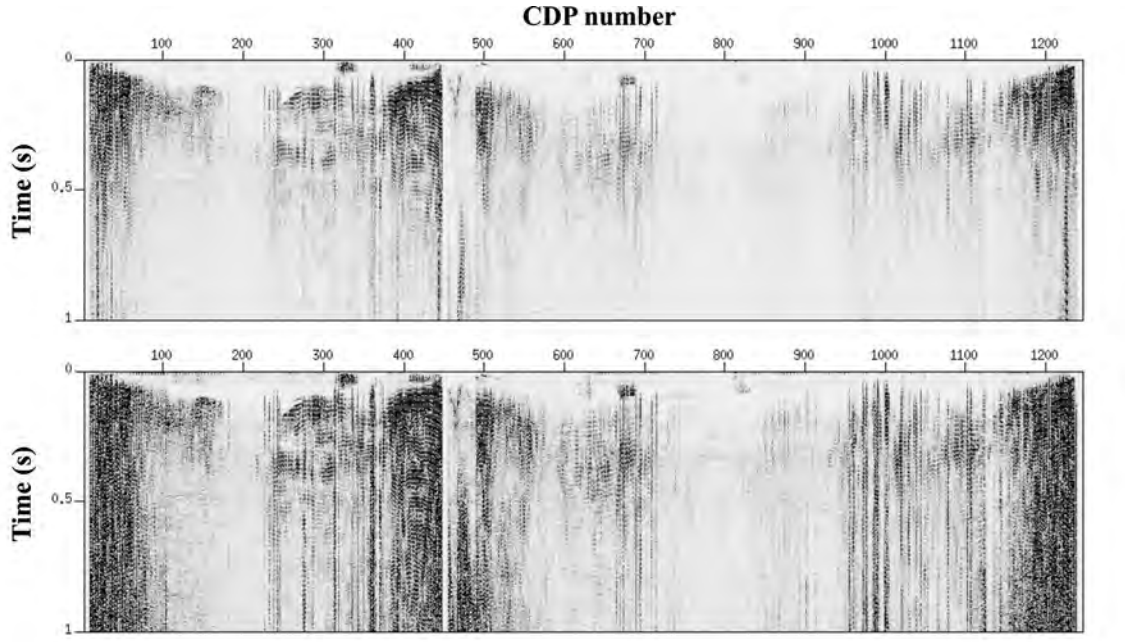

Fig. 3 - P- (top) and S-wave (bottom) velocity reflectivity sections along the Line 2 (see text).

3.2. The results

The AVO inversion was applied to all 2D and 3D seismic data sets. Note that the reliability of the result depends on the data quality and the coverage of the seismic data. Examples of the reflectivity sections obtained are reported in Figs. 3 and 4, which show 2D and 3D, data respectively. In general, comparing the P and S reflectivity sections, it is possible to discriminate between the reflections caused mainly by geological features and the reflections that can be attributed to fluid content variation. In this case, we can identify the same main reflectors in both P and S reflectivity sections (Figs. 3 and 4), already detected in the stacked sections (Giustiniani *et al.*, 2009), because of the geological characteristics of the aquifer system (Giustiniani *et al.*, 2009). Nevertheless, to avoid a misinterpretation of the results, we have calculated the ratio between the P- and S-wave reflectivity sections (Fig. 5).

The comparison of the results shows that the AVO analysis of seismic data acquired in different seasons detects the same features. As revealed by the measured and modelled velocities (see section 2), the seismic data cannot detect any changes in the water saturation and pore pressure inside the aquifers related to the seasonal change.

In this paper, we show, in detail, the results obtained from the 2D Line 2, for which the AVO analysis gives the best results because of the quality and the coverage of the data. The two main aquifers are identified by the strong Poisson ratio variation (Fig. 5). We blanked the area where the AVO inversion is not reliable, i.e. the areas where the curve fitting is suspect, due to noise or insufficient aperture. Note also the high contrast at about 500 m depth, possibly related to lithological changes that may reflect another aquifer.

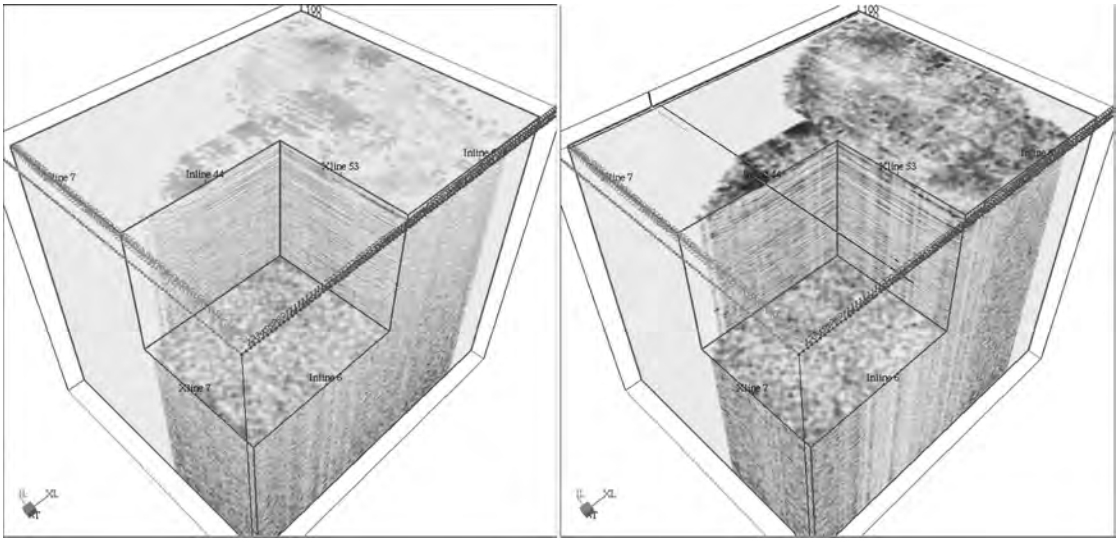

Fig. 4 - P- (left) and S-wave (right) velocity reflectivity sections along the 3D cube 3 after AVO inversion (see text).

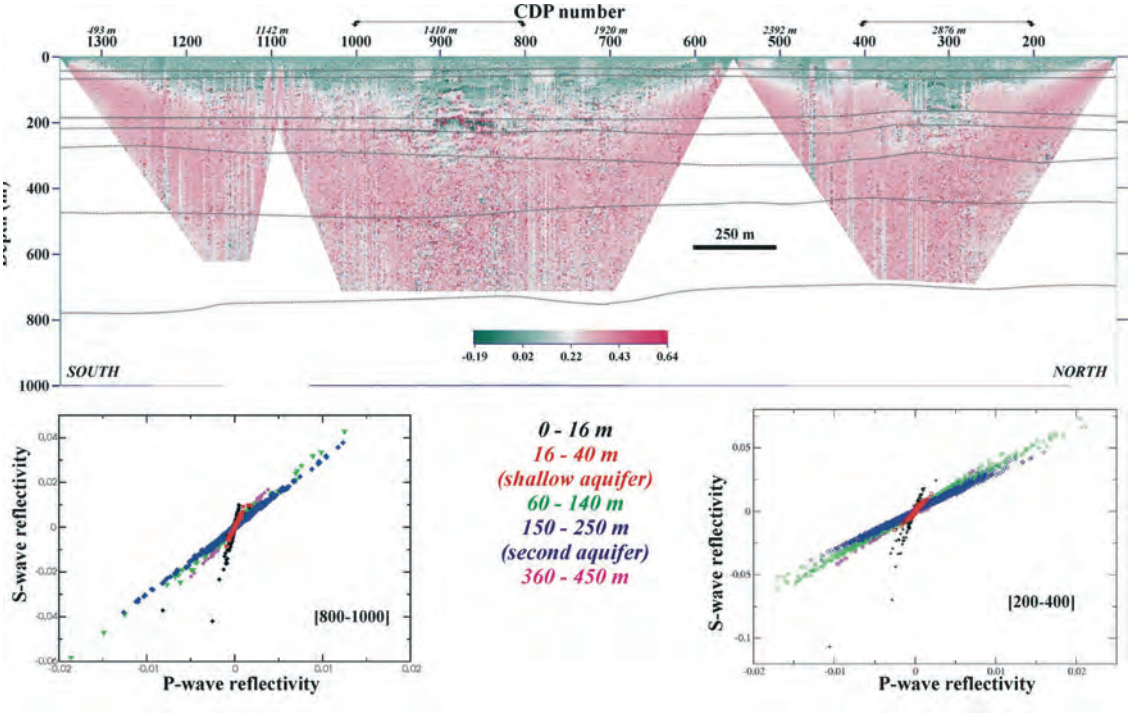

Fig. 5 - Top: P to S wave velocity reflectivity section; the arrowed lines indicate the area where the cross-plots are evaluated. The thin lines indicate the main reflectors identified in the staked section and inverted to obtain tomographic velocity. Bottom: P- versus S-wave velocity reflectivities at selected CDP intervals.

Finally, we evaluated the cross-plots of P and S velocity versus reflectivity, to verify if different petro-physical characteristics versus depth can be detected along the seismic profiles. To this end, we selected two areas where the coverage is high enough to guarantee a reliable AVO inversion, i.e., between Common Depth Points (CDPs) 200 to 400 and 800 to 1000 (Fig. 5). To detect different trends, we considered the following depth intervals:

1) shallow part (between 0 and 16 m; in black);
2) first aquifer (between 16 and 40 m; in red);
3) intermediate part between the two main aquifers (between 60 and 140 m; in green);
4) the second aquifer (between 150 and 250 m; in blue);
5) depth greater than 250 m (between 360 and 450 m; in magenta).

The two selected zones produce similar results. The two main aquifers have different cross-plots compared to the other layers. The deepness, i.e. the relationship between P- and S-wave velocity contrasts, decreases versus depth, even if the characteristics of the layers between the two aquifers and below the deeper one are similar.

4. The density and porosity maps

The velocity (V) was translated in terms of density (ρ) by using the well-known Gardner relationship (Gardner *et al.*, 1974), as used for the AVO analysis (see section 3):

$$\rho = 0.31V^{0.25}. \tag{4}$$

Supposing that the density of the matrix (ρ_s) is about 2600 kg/m^3 and that one of the water one (ρ_w) is about 1000 kg/m^3, we obtain the following relationship between density and porosity (Φ), i.e. water saturation:

$$\phi = \frac{\rho_s - \rho}{\rho_s - \rho_w}. \tag{5}$$

The results show that the shallowest confined aquifer is characterized by a density of about 1900 kg/m^3 and a porosity of about 36-40%. The second aquifer, located at about 180 m depth, is well imaged because it shows a higher porosity (equal to about 32%) with respect to the upper layer, characterized by a porosity of about 28%. Note that the deeper aquifer presents a porosity of about 33%. Regarding the density, the deep aquifers are characterized by a density of about 2100 kg/m^3.

The velocity, density and porosity models are interpolated in order to obtain a complete 3D model of the Torrate area by using a commercial software. We assumed a cell size of 20(x)·20(y)·25(z) m and a number of cells equal to 198, 211, and 23 along the three directions respectively.

The data were interpolated by using the inverse distance algorithm (Franke, 1982; Davis, 1986). The inverse distance method is a weighted average interpolator that can be either an exact

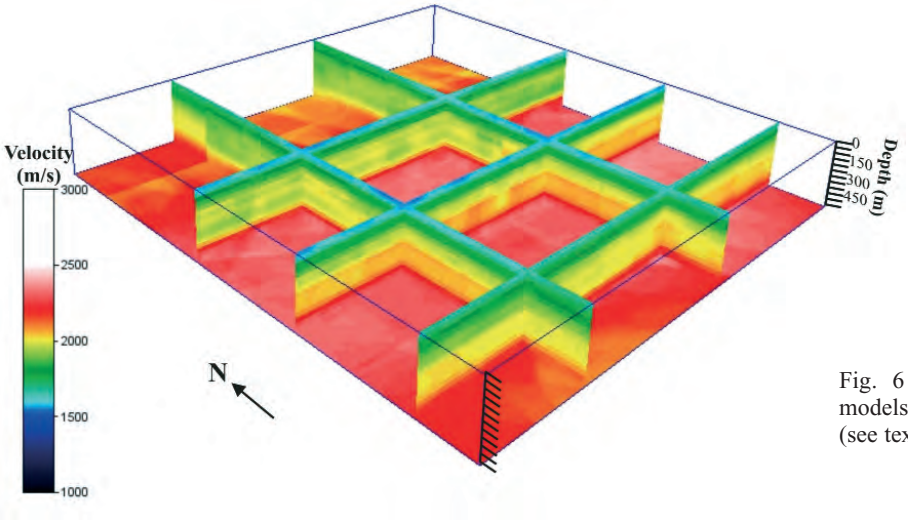

Fig. 6 - 3D velocity (m/s) models after the interpolation (see text).

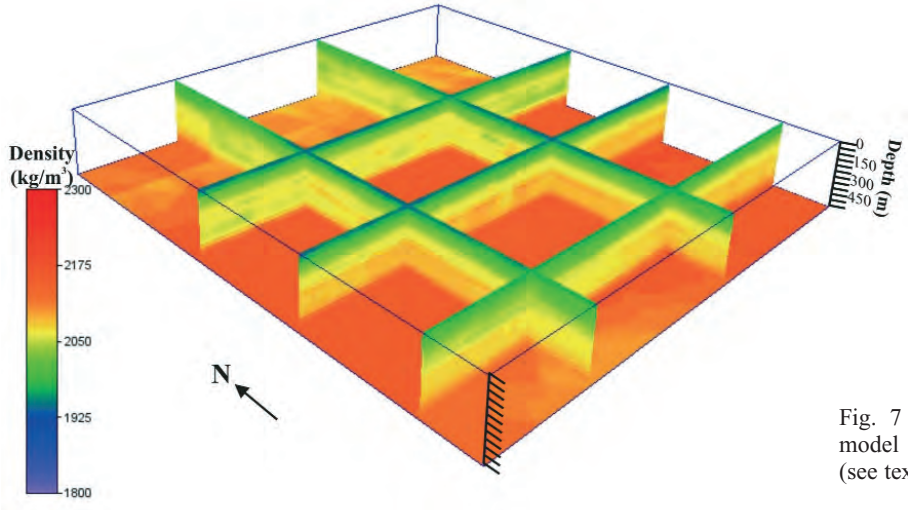

Fig. 7 - 3D density (kg/m^3) model after the interpolation (see text).

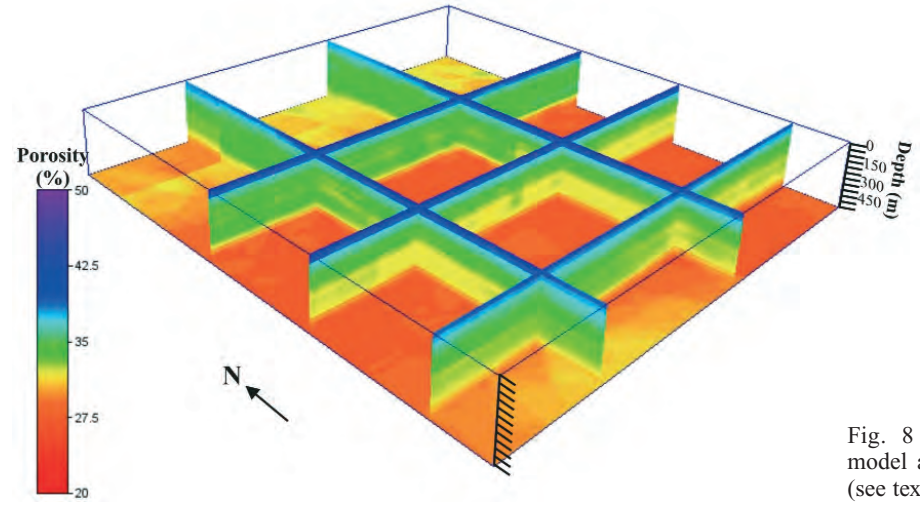

Fig. 8 - 3D porosity (%) model after the interpolation (see text).

or a smoothing interpolation.

We applied the interpolator module to all data sets obtaining velocity, density and porosity distribution. The results are reported in Figs. 6 to 8, where the depth ranges from 0 to 550 m. The 3D models indicate that the area has variable characteristics, with strong lateral velocity variations that suggest changes in the interfaces, geometry and the aquifer system thickness. The analyses of these data confirm an increase of porosity and the thickness of aquifers northwards in accordance with the other data acquired in the frame of the CAMI project (Giustiniani *et al.* 2009).

5. Conclusions

The results obtained from the AVO analysis confirm the presence of a shallow aquifer (at about 30 m) and a deeper one (at about 180 m). In particular, the cross-plots of the P and S velocity versus reflectivity show different trends, being related to fluid contents and lithologic changes. Moreover, seismic data cannot detect the pore pressure condition in this area, but provided information about the geometrical structures and the petro-physical properties of the aquifers.

The velocity fields, that were obtained as described in Giustiniani *et al.* (2009) and Picotti *et al.* (2009), were translated in terms of porosity and density by using empirical relationships. The obtained porosity and density maps show the main increase of aquifer thickness versus north and a stronger variability of the petro-physical characteristics of two shallower aquifers than the deeper ones.

Acknowledgments. We are very grateful to Elvio Del Negro for his contribution and technical support in collecting the field data. We acknowledge the European Community that has supported this project (LIFE Project Number - LIFE04 ENV/IT/000500). We wish to thank the Acquedotto Basso Livenza, and in particular Enrico Marin, for the logistical support and all the information provided (hydrogeological data and the stratigraphies of the catchment wells).

REFERENCES

Accaino F., Tinivella U., Rossi G. and Nicolich R.; 2005: *Geofluid evidence from analysis of deep crustal seismic data (Southern Tuscany, Italy).* Journal of Volcanology and Geothermal Research, **148**, 46–59.

Aki K. and Richards P.G.; 1980: *Quantitative seismology: Theory and methods.* W.H. Freeman, San Francisco, 932 pp.

Bourbié T., Coussy O. and Zinzner B.; 1987: *Acoustics of Porous Media.* Gulf Publishing, Houston, Texas, 56 pp.

Davis J.C.; 1986: *Statistics and Data Analysis in Geology.* John Wiley and Sons, New York, NY, 646 pp.

Franke R.; 1982: *Scattered Data Interpolation: Test of Some Methods.* Mathematics of Computations, **33**, 181-200.

Gardner G.H.F., Gardner L.W. and Gregory A.R.; 1974: *Formation velocity and density – The diagnostic basics for stratigraphic traps.* Geophysics, **39**, 770-780.

Giustiniani M., Accaino F., Del Negro E., Picotti S. and Tinivella U.; 2009: *Characterisation of shallow aquifers by 2D*

high-resolution seismic data analysis. Boll. Geof. Teor. Appl., **50**, 29-38.

Picotti S., Giustiniani M., Accaino F. and Tinivella U.; 2009: *Depth modelling and imaging of the 4D seismic survey of the Basso Livenza area (NE Italy).* Boll. Geof. Teor. Appl., **50**, 71-82.

Prasad A. and Meissner G.; 1992: *Attenuation mechanism in sands: Laboratory versus theoretical (Biot) data.* Geophysics, **57**, 710-719.

Prasad M., Zimmer M.A., Berge P.A. and Bonner B.P.; 2004: *Laboratory measurements of velocity and attenuation in sediments.* Lawrence Livermore National Laboratory Report, UCRL-JRNL-205155.

Schön S.; 1996: *Physical properties of rocks-Fundamentals and principles of petrophysics.* Handbook of Geophysical Exploration: Seismic Exploration, vol. 18, Pergamon, Oxford, UK; Tarrytown, N. Y., 583 pp.

Vern R. and Hilterman F.; 1995: *Lithology color-coded seismic sections: The calibration of AVO crossplotting of rock properties.* The Leading Edge, **14**, 847-853.

Corresponding author: Umberta Tinivella
Dipartimento Geofisica della Litosfera
Istituto Nazionale Oceanografia e di Geofisica Sperimentale
Borgo Grotta Gigante 42/c, Sgonico (Trieste), Italy
phone: +39 040 2140219; fax: +39 040 327307; e-mail: utinivella@inogs.it